Rapid Communications

Ultrafast depinning of domain walls in notched antiferromagnetic nanostructures

Z. Y. Chen,[1] M. H. Qin,[1,*] and J.-M. Liu[2]

[1]*Institute for Advanced Materials, South China Academy of Advanced Optoelectronics and Guangdong Provincial Key Laboratory of Quantum Engineering and Quantum Materials, South China Normal University, Guangzhou 510006, China*

[2]*Laboratory of Solid State Microstructures and Innovative Center for Advanced Microstructures, Nanjing University, Nanjing 210093, China*

(Received 8 May 2019; published 3 July 2019)

The pinning/depinning of an antiferromagnetic (AFM) domain wall is certainly the core issue for AFM spintronic device operation. In this work, we study theoretically the Néel-type domain wall pinning/depinning at a notch in an AFM nanostructure (nanoribbon). The depinning field depending on the notch dimension and intrinsic material properties is deduced and also numerically calculated. Contrary to conventional conception, it is revealed that the depinning field is remarkably dependent on the damping constant and the time-dependent oscillation of domain wall position in the weakly damping regime benefits to the wall depinning, resulting in a gradual saturation of the depinning field with increasing damping constant. A one-dimensional model accounting of the internal dynamics of the domain wall is used to explain perfectly the simulated results. It is demonstrated that the depinning mechanism of an AFM domain wall differs from the ferromagnetic domain wall by exhibiting a depinning typically three orders of magnitude faster than the latter, unveiling another origin for ultrafast dynamics of an AFM system.

DOI: 10.1103/PhysRevB.100.020402

Antiferromagnetic (AFM) materials are promising for the next generation of spintronic devices and attract substantial attention because they have strong anti-interference capability and promise ultrafast magnetic dynamics [1–8]. As a frontier and highly concerning issue for advanced spintronics, the domain wall dynamics of antiferromagnets is under extensive investigation. Specifically, several stimuli have been proposed to drive the domain wall motion, including the Néel spin-orbit torques [9,10], spin waves [11,12], temperature gradients [13–15], spin waves, elastic waves, and microwaves [16–18]. These works provide useful information for future AFM storage device design.

Nevertheless, most of these works discuss models for perfect samples and the wall pinning caused by disorder and local defects is neglected. As a matter of fact, the wall pinning may play an important role in magnetic dynamics. On one hand, for a realistic spintronic device where inhomogeneity and lattice defects are inevitable, the wall dynamics could be significantly affected and the wall pinning/depinning becomes the limited step for device operation. For example, it was reported that electrical-current-induced switching of AFM domains in CuMnAs occurs only in localized regions, strongly suggesting the important role of wall pinning [19]. Given these reasons, a clarification of the underlying mechanisms for wall pinning/depinning becomes emergent. On the other hand, artificial lattice defects such as notches with proper shape could be used in discretizing domain wall position and enhancing its stability against thermal fluctuations and stray fields in potential race-track memory and logic devices [20–24]. Therefore, the dynamics of AFM domain wall pinning/depinning appears to be one of the core issues for application potentials and basic research of AFM spintronics.

Fortunately, the wall pinning in ferromagnetic systems has been extensively investigated, and the accumulated experience can be a reference for the AFM domain dynamics study [25–32]. For a ferromagnetic wall, the depinning field can be analytically obtained by minimizing the total energy, demonstrating the critical role of notch geometry in pinning the wall [26]. More interestingly, the dependence of the depinning field on the Gilbert damping for a ferromagnetic system has been revealed in micromagnetic simulations, and the damping constant, if small, can reduce the depinning field, contrary to general expectation that they should be independent of each other [27]. This phenomenon not only reveals the complexity of domain wall pinning, but more importantly provides a method of domain wall manipulation. However, as far as we know, few works on the pinning/depinning of an AFM domain wall have been available, although this issue is certainly more important than and distinctly different from the case of a ferromagnetic wall.

In the following, we discuss the domain wall pinning/depinning for an AFM nanostructure with a notch, without losing the generality, while the calculation methods and main conclusions apply to antiferromagnets with other lattice defects. For simplicity, we consider a nanoribbon and the notch has a rectangular section, as shown in Fig. 1(a). We can derive the depinning field h_{dep} as a function of the notch size and uniaxial anisotropy in a simplified framework and the theory agrees well with numerical simulations in the large damping regime. Moreover, it will be shown that the depinning field gradually increases to a saturation value with increasing damping constant, and this prediction allows one to modulate the damping constant through an elaborate material design, so that the domain wall depinning can be in turn

*qinmh@scnu.edu.cn

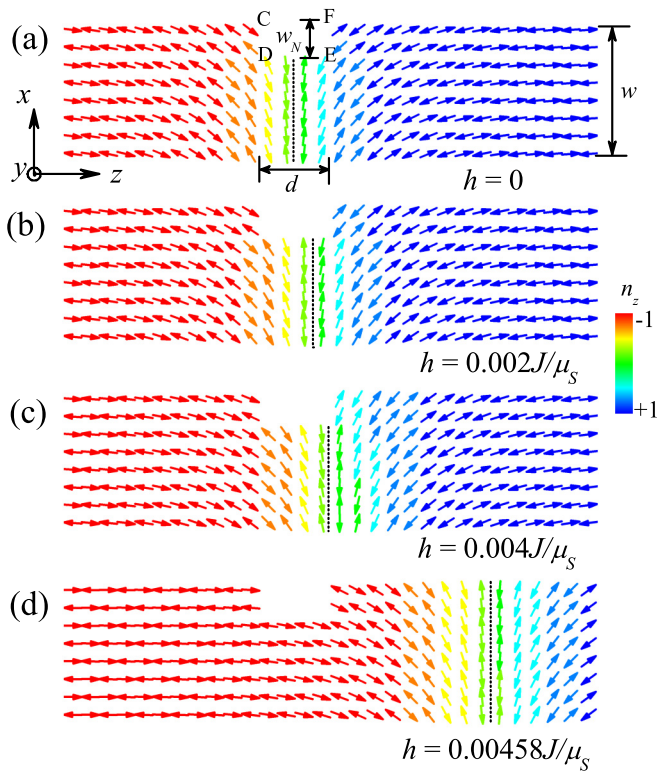

FIG. 1. Equilibrium spin structures around the notch in the AFM nanoribbon with lattice sizes $l \times w \times t_l$ under (a) $h = 0$, (b) $h = 0.002\,J/\mu_S$, (c) $h = 0.004\,J/\mu_S$, and (d) $h = 0.00458\,J/\mu_S$. The color represents the magnitude of the z component of the staggered magnetization n_z, and the position of the domain wall center is depicted by the black dashed lines.

effectively controlled. In order to understand the underlying physics better, we perform the analytical calculation based on the one-dimensional model, which reveals the important role of the internal domain wall dynamics. Our work also addresses the depinning mechanism for an AFM wall different from a ferromagnetic wall. This new mechanism allows the depinning speed to be typically three orders of magnitude higher than that for a ferromagnetic wall depinning.

We start from the domain wall pinning at a rectangular notch for an AFM nanoribbon. This nanoribbon is geometrically defined by length l along the z axis, width w, and thickness t_l, as shown in Fig. 1. We discuss the scenario of current-induced Néel spin-orbit torques (or staggered effective field), as demonstrated in CuMnAs and Mn_2Au for driving the domain wall motion, i.e., the wall is typically of the Néel type [6,8,9]. For this scenario, the model Hamiltonian is given by [33,34]

$$H = \frac{A_0}{2}\mathbf{m}^2 + \frac{A}{2}\nabla\mathbf{n}\cdot\nabla\mathbf{n} + L_0\mathbf{m}\cdot\nabla\mathbf{n} - \frac{K_z}{2}n_z^2 + \gamma\rho h n_z, \tag{1}$$

where $A_0 = 4JS^2/a$ is the homogeneous exchange constant with AFM coupling $J > 0$, spin length S, and lattice constant a, $\mathbf{m}$ is the total magnetization $\mathbf{m} = (\mathbf{m}_1 + \mathbf{m}_2)/2S$ with $\mathbf{m}_1$ and $\mathbf{m}_2$ the AFM sublattice magnetizations, $A = 2aJS^2$ is the inhomogeneous exchange constant, $\mathbf{n}$ is the staggered magnetization $\mathbf{n} = (\mathbf{m}_1 - \mathbf{m}_2)/2S$, $L_0 = 2JS^2$ is the parity-breaking parameter, $K_z = 2K_0S^2/a$ is the anisotropy constant along the z axis in the continuum model with anisotropy constant K_0 in the discrete model, γ is the gyromagnetic ratio, $\rho = S\hbar/a$ is the density of the staggered spin angular momentum per unit cell, h is the staggered effective field, and n_z is the z component of $\mathbf{n}$. Here, the notch has its width d and depth w_N, as depicted in Fig. 1(a).

Noting that $\mathbf{m}$ is just a slave variable of $\mathbf{n}$ [33], and we eliminate $\mathbf{m}$ by $\mathbf{m} = -L_0\nabla\mathbf{n}/A_0$ and obtain

$$H = \frac{A^*}{2}\nabla\mathbf{n}\cdot\nabla\mathbf{n} - \frac{K_z}{2}n_z^2 + \gamma\rho h n_z, \tag{2}$$

where $A^* = A - L_0^2/A_0$ is the effective exchange constant. As shown in the Supplemental Material A for the detailed derivation [35], the depinning field $h_{\rm dep}$, based on this Hamiltonian model, can be solved strictly after a similar derivation [26]

$$h_{\rm dep} = \frac{2K_0/\mu_S}{2w/w_N - 1}, \tag{3}$$

where μ_S is the saturation moment. It is noted that for a nanoribbon, the depinning field is independent of thickness. As clearly indicated in Eq. (3), $h_{\rm dep}$ depends on several parameters including the anisotropy constant K_0 and the w/w_N ratio. Thus, the devices with various depinning fields could be designed through modulating ratio w/w_N and/or choosing appropriate materials.

In order to check the validity of Eq. (3), we also perform the numerical simulations based on the atomistic Landau-Lifshitz-Gilbert (LLG) equation [14],

$$\frac{\partial\mathbf{S}_i}{\partial t} = -\frac{\gamma}{(1+\alpha^2)}\mathbf{S}_i \times [\mathbf{H}_i + \alpha(\mathbf{S}_i \times \mathbf{H}_i)], \tag{4}$$

where $\mathbf{S}_i$ is the normalized atomic spin at site i, α is the damping constant, and $\mathbf{H}_i = -\mu_s^{-1}\partial H/\partial\mathbf{S}_i$ is the effective field. Without loss of generality, $l = 120\,a$, $t_l = a$, $w = 8a$, $K_0 = 0.02\,J$, $d = 4a$, $w_N = 2a$, and $\alpha = 0.02$ are selected.

Figure 1 presents the spin structures of the nanoribbon for various h. Here, the Néel-type AFM domain wall is pinned at the notch at $h = 0$ and the spin configuration is symmetric around the notch due to the absence of chirality, as shown in Fig. 1(a). The spins on the wall midplane are aligned in parallel to the x axis and perpendicular to those spins inside the AFM domains aside. When a small h is applied along the z axis, the wall slightly shifts toward the right side, as seen from the delicate change of the spin configuration. With increasing h, those spins on the left side of the notch midplane tend to rotate toward the negative z axis while those on the right side of the notch midplane tend to rotate toward the x axis, as shown in Figs. 1(b) and 1(c), a consequence of the wall depinning from the notch. The wall depinning becomes clear in Fig. 1(c) where the wall midplane deviates clearly from the notch midplane. The spin configuration after the full wall depinning from the notch is shown in Fig. 1(d).

Subsequently, we investigate the dependences of $h_{\rm dep}$ on the notch geometry and several physical parameters including the anisotropy and damping constants. The calculated curves (analytical) from Eq. (3) plus the simulated results (numerical) based on the LLG dynamics, Eq. (4), for different values of notch depth w_N, nanoribbon thickness w, anisotropy constant

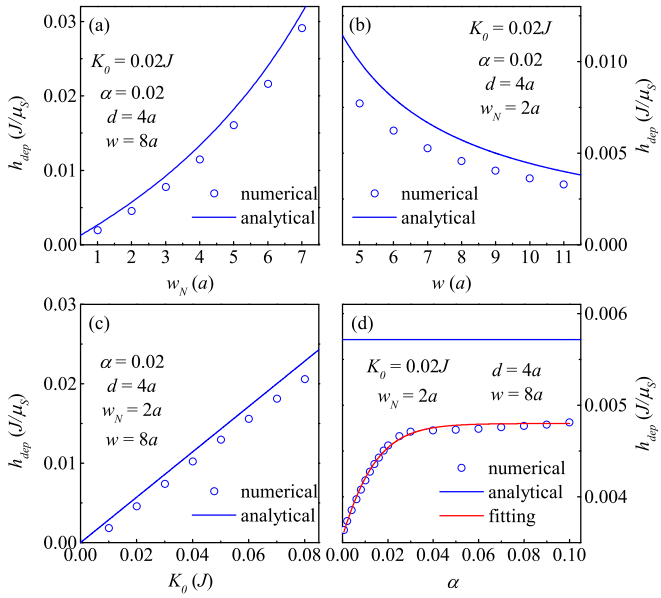

FIG. 2. Numerical (empty circles) and analytical (blue solid line) calculated depinning field as a function of (a) the depth of the notch w_N, (b) the width of the nanoribbon w, (c) the anisotropy constant K_0, and (d) the damping constant α. The red solid line in (d) is the fitting results based on Eq. (14).

K_0, and damping constant α are plotted in Figs. 2(a)–2(d), respectively. Several features deserve highlighting here. First, the model calculated curves and numerically simulated data on dependences $h_{\rm dep}(w_N)$, $h_{\rm dep}(w)$, and $h_{\rm dep}(K_0)$ respectively show qualitatively similar tendencies, suggesting that Eq. (3) can describe roughly these dependences although a quantitative difference between the model and simulation appears for each dependence. Second, a qualitative difference between the model and simulation appears for function $h_{\rm dep}(\alpha)$, as shown in Fig. 2(d). While the model suggests independence of $h_{\rm dep}$ on damping constant α, the numerical simulation reveals that $h_{\rm dep}$ is remarkably dependent on α in the small α regime. $h_{\rm dep}$ shows a gradual growth with α until the large α regime where $h_{\rm dep}$ becomes saturated, i.e., independent of α in the large damping regime. The difference between Eq. (3) and simulated results for $h_{\rm dep}(\alpha)$ is understandable since the LLG damping is a time-dependent effect. It is noted that the internal dynamics of the domain wall is completely neglected in deriving Eq. (3), while this dynamics becomes particularly remarkable in the small α regime where the time-dependent spin oscillation can be significant due to the weak damping. Actually, the damping constants in typical AFM materials including Mn_2Au and NiO [36] have been confirmed to be $\sim 10^{-3}$. Therefore, the model prediction Eq. (3) becomes invalid and the underlying physics should be reconsidered.

In order to uncover the intriguing physics, we need to track the domain wall evolution. In proceeding, we first define the position of a domain wall. Similar to the well-studied skyrmions, the position of a domain wall is estimated by $q(t)$ [37]:

$$q = \frac{\int z(1-|n_z|)dx\,dz}{\int (1-|n_z|)dx\,dz}, \tag{5}$$

where q is the coordinate of the wall midplane. Given this definition, one starts with the one-dimensional model with inclusion of the internal dynamics of domain wall motion [28,29]. The Hamiltonian density for this model reads [33]

$$H_{\rm 1D} = \frac{A_0}{2}\mathbf{m}^2 + \frac{A}{2}(\partial_z \mathbf{n})^2 + L_0\mathbf{m}\cdot\partial_z\mathbf{n} - \frac{K_z}{2}n_z^2 + \gamma\rho h n_z + V(z), \tag{6}$$

where the pinning effect from the notch is described by potential energy $V(z)$.

Subsequently, we study the Lagrangian density $L = K - H_{1D}$ with $K = \rho\mathbf{m}\cdot(\dot{\mathbf{n}}\times\mathbf{n})$ is the kinetic energy term introduced by the Berry phase, and $\dot{\mathbf{n}}$ represents the derivative with respect to time [33,38,39]. Then, we eliminate $\mathbf{m}$ with $\mathbf{m} = (\rho\dot{\mathbf{n}}\times\mathbf{n} - L_0\partial_z\mathbf{n})/A_0$ [33], and obtain

$$L = \frac{\rho^2}{2A_0}\dot{\mathbf{n}}^2 - \frac{A^*}{2}(\partial_z\mathbf{n})^2 + \frac{K_z}{2}n_z^2 - \gamma\rho h n_z - V(z). \tag{7}$$

It is noted that the Rayleigh function density $R = \alpha\rho\,\dot{\mathbf{n}}^2/2$ is introduced into the Lagrangian formalism in order to describe the dissipative dynamics [38,39]. Following the earlier work, we assume a robust domain wall structure which can be described by $\mathbf{n} = [\mathrm{sech}[(z-q)/\lambda]\cos\Phi,\ \mathrm{sech}[(z-q)/\lambda]\sin\Phi,\ \tanh[(z-q)/\lambda]$ [38], where the azimuthal angle Φ of the wall is introduced as the collective coordinates. After substituting the domain wall ansatz and applying the Euler-Lagrange equation, we obtain the equation of motion for variables q and Φ,

$$\frac{\rho^2}{\lambda A_0}\ddot{q} + \frac{\alpha\rho}{\lambda}\dot{q} + \frac{d\varepsilon}{dq} - \gamma\rho h = 0 \tag{8}$$

and

$$\frac{\rho^2}{A_0}\ddot{\Phi} + \alpha\rho\dot{\Phi} = 0. \tag{9}$$

It is noted that the first term in Eq. (8) describes the wall inertia and other terms represent the forces exerted respectively by the damping α, pinning potential $\varepsilon(q)$, and current-induced effective magnetic field h. By substituting the initial condition $\Phi(0) = d\Phi/dt|_{t=0} = 0$ into Eq. (9), one obtains $\Phi(t) = 0$, consistent with the fact that an AFM domain wall is confined in the easy plane due to the antiparallel arrangement of neighboring spins.

For simplicity, we assume a parabolic potential [23,29]

$$\varepsilon(q) = \begin{cases} K_N q^2/2 & (|q| < L_N) \\ K_N L_N^2/2 & (|q| \geqslant L_N) \end{cases}, \tag{10}$$

where K_N is the elastic constant and L_N is the radius of the potential well. After substitutions and necessary simplification, the equation of motion for q is updated to

$$\ddot{q} + G\dot{q} + \omega_N^2 q - h_N = 0, \tag{11}$$

where $G = aA_0/\rho$, $h_N = \gamma A_0\lambda h/\rho$, and $\omega_N = (\lambda A_0 K_N/\rho^2)^{1/2}$ is the natural angular frequency of the free harmonic oscillator. Here, we can see the existence of domain wall oscillation if damping constant α is small. This

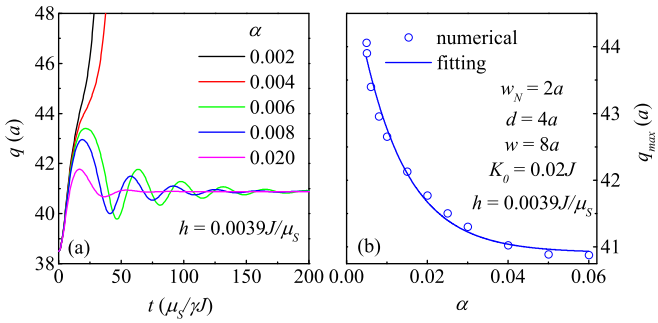

FIG. 3. (a) The domain wall position as a function of time for various damping constants under $h = 0.0039\,J/\mu_S$. (b) Numerical (empty circles) and analytical (solid line) calculated maximum displacement of the domain wall as a function of α under $h = 0.0039\,J/\mu_S$.

oscillation is the major reason for the invalid prediction of the depinning field by Eq. (3).

Noting that Eq. (11) describes the damping oscillation of a domain wall, one has the solution for $\alpha < \alpha_c = 2\rho^2 a\omega_N/JA_0$ representing the underdamped oscillation:

$$q(t) = e^{-Gt}(C_1 \cos\omega_p t + C_2 \sin\omega_p t) + h_N/\omega_N^2, \qquad (12)$$

where $\omega_p = (\omega_N^2 - G^2/4)^{1/2}$ is the oscillating angular frequency of the wall, and C_1, C_2 are integral constants depending on the initial condition.

For better illustration, the simulated $q(t)$ curves based on the LLG equation at various damping constant α are plotted in Fig. 3(a), benefiting the discussion. For $\alpha > 0.005$, one observes the domain wall oscillation around the equilibrium position with an attenuating amplitude. Moreover, the oscillation amplitude is enhanced with decreasing α. Finally, for $\alpha < 0.005$, when the maximum displacement of the wall oscillation, defined as $|\Delta q|_{\max} = |q(t) - q(0)|_{\max}$, exceeds the height of the pinning potential [29], the wall would successfully depin from the notch and propagates freely along the nanoribbon, as clearly shown in the Supplemental Material movie [35].

As demonstrated in Eq. (12), the displacement of the wall oscillation consists of the oscillatory part (A_S) and stationary part (q_{eq}) [29], and its maximum value is approximately given by

$$|\Delta q|_{\max} = A_S + q_{eq} = e^{-G\arctan(C_2/C_1)/\omega_p}\sqrt{C_1^2 + C_2^2} + h_N/\omega_N^2, \qquad (13)$$

where $\omega_p \approx \omega_N$ is obtained for $\alpha < \alpha_c$. In this case, since $|\Delta q|_{\max}$ decreases exponentially with α, a larger external field is required to generate the wall displacement for the wall depinning. As $|\Delta q|_{\max} > L_N$, the wall eventually depins from the notch.

Noting that the pinning potential parameters including K_N and L_N are unknown, we need a reasonable estimation of them by fitting the simulated results based on Eq. (13). As shown in Fig. 3(b) where the simulated furthest position of the domain wall, $q_{\max}$, as a function of α, is plotted. The excellent fitting of the simulated data by Eq. (13), on the other hand, further confirms the validity of our theory.

Since the oscillating amplitudes C_1 and C_2 are proportional to external or current-induced staggered field h, one can introduce the field-independent parameters $c_1 = C_2/C_1$, $c_2 = ({C_1}^2 + {C_2}^2)^{1/2}/h$ for brevity. Subsequently, the depinning field under the condition $|\Delta q|_{\max} = L_N$ is obtained:

$$h_{\rm dep} = \frac{L_N}{e^{-G\arctan c_1/\omega_p}c_2 + \gamma\rho/K_N}. \qquad (14)$$

A similar fitting approach can be used to estimate L_N. As shown in Fig. 2(d), the simulated results coincide very well with Eq. (14) with one adjustable variable L_N, demonstrating the important role of the domain wall oscillation in the domain wall depinning. Such an oscillation behavior is one character of the internal dynamics for an AFM nanoribbon with a notch.

Finally, we would like to address the significance of the present results. It is known that the performance of domain wall based race-track memory not only depends on the wall motion velocity, but also relies on the wall depinning time. It is clearly shown here that an AFM domain wall depinning is distinctly different from that of a ferromagnetic domain wall. For a ferromagnetic nanoribbon, the wall oscillation is related to the wall internal angle which is mainly determined by the internal fields including magnetocrystalline anisotropy and Dzyaloshinskii-Moriya (DM) exchange [27]. Generally, the depinning time is inversely proportional to the magnitude of internal fields and has a typical value of ~1.0 ns [22–24,27]. However, for an AFM system, the wall oscillation stems from the second-order derivative of domain wall position q with respect to time rather than the azimuthal angle, as clearly illustrated in Eq. (8). Since the derivative originates from the strong AFM exchange interaction between two sublattices, which is about three orders larger than the anisotropy and DM exchange, one is sure that the depinning time for such an AFM domain wall should be three orders of magnitude shorter than a ferromagnetic one. It implies a surprisingly short depinning time of ~0.001 ns for CuMnAs with the Néel temperature $T_N \approx 480$ K, $a \approx 3.8$ Å, and $\mu_S \approx 3.6\,\mu_B$ [40], where μ_B is the Bohr magneton. While it is well believed that the AFM domain switching is faster than ferromagnetic domain switching, the present work presents a quantitative estimation of the domain wall depinning time, directly evidencing this well-believed but not yet well-evidenced claim.

In conclusion, we have studied theoretically the domain wall depinning at a notch in an AFM nanostructure (nanoribbon). The depinning field depending on the notch dimension and intrinsic physical parameters are derived theoretically and also simulated based on the LLG equation. The remarkable dependence of the depinning field on the damping constant is revealed, which is attributed to the time-dependent oscillation of the domain wall in the small damping regime. A one-dimensional model considering the internal dynamics of a domain wall is sufficiently investigated to explain perfectly the simulated results. More importantly, our work unveils the different depinning mechanism of an AFM domain wall from a ferromagnetic domain wall, which may result in a depinning speed typically three orders faster than the latter, and thus provide a physical basis for the ultrafast dynamics of an AFM system.

We sincerely appreciate the insightful discussions with Zhengren Yan, Yilin Zhang, and Huaiyang Yuan. The work is supported by the National Key Projects for Basic Research of China (Grant No. 2015CB921202), the Natural Science Foundation of China (Grant No. 11204091), the Science and Technology Planning Project of Guangzhou in China (Grant No. 201904010019), and the Natural Science Foundation of Guangdong Province (Grant No. 2016A030308019).

[1] O. Gomonay, V. Baltz, A. Brataas, and Y. Tserkovnyak, Nat. Phys. **14**, 213 (2018).
[2] A. V. Kimel, B. A. Ivanov, R. V. Pisarev, P. A. Usachev, A. Kirilyuk, and Th. Rasing, Nat. Phys. **5**, 727 (2009).
[3] N. Thielemann-Kühn, D. Schick, N. Pontius, C. Trabant, R. Mitzner, K. Holldack, H. Zabel, A. Föhlisch, and C. Schußler-Langeheine, Phys. Rev. Lett. **119**, 197202 (2017).
[4] M. J. Grzybowski, P. Wadley, K. W. Edmonds, R. Beardsley, V. Hills, R. P. Campion, B. L. Gallagher, J. S. Chauhan, V. Novak, T. Jungwirth, F. Maccherozzi, and S. S. Dhesi, Phys. Rev. Lett. **118**, 057701 (2017).
[5] I. Fina, X. Martí, D. Yi, J. Liu, J. H. Chu, C. R. Serrao, S. Suresha, A. B. Shick, J. Železný, T. Jungwirth, J. Fontcuberta, and R. Ramesh, Nat. Commun. **5**, 4671 (2014).
[6] P. Wadley, B. Howells, J. Železný, C. Andrews, V. Hills, R. P. Campion, V. Novák, K. Olejník, F. Maccherozzi, S. S. Dhesi, S. Y. Martin, T. Wagner, J. Wunderlich, F. Freimuth, Y. Mokrousov, J. Kuneš, J. S. Chauhan, M. J. Grzybowski, A. W. Rushforth, K. W. Edmonds, B. L. Gallagher, and T. Jungwirth, Science **351**, 587 (2016).
[7] X. Z. Chen, R. Zarzuela, J. Zhang, C. Song, X. F. Zhou, G. Y. Shi, F. Li, H. A. Zhou, W. J. Jiang, F. Pan, and Y. Tserkovnyak, Phys. Rev. Lett. **120**, 207204 (2018).
[8] J. Železný, H. Gao, K. Výborný, J. Zemen, J. Mašek, A. Manchon, J. Wunderlich, J. Sinova, and T. Jungwirth, Phys. Rev. Lett. **113**, 157201 (2014).
[9] O. Gomonay, T. Jungwirth, and J. Sinova, Phys. Rev. Lett. **117**, 017202 (2016).
[10] Y. L. Zhang, Z. Y. Chen, Z. R. Yan, D. Y. Chen, Z. Fan, and M. H. Qin, Appl. Phys. Lett. **113**, 112403 (2018).
[11] E. G. Tveten, A. Qaiumzadeh, and A. Brataas, Phys. Rev. Lett. **112**, 147204 (2014).
[12] A. Qaiumzadeh, L. A. Kristiansen, and A. Brataas, Phys. Rev. B **97**, 020402(R) (2018).
[13] S. K. Kim, O. Tchernyshyov, and Y. Tserkovnyak, Phys. Rev. B **92**, 020402(R) (2015).
[14] S. Selzer, U. Atxitia, U. Ritzmann, D. Hinzke, and U. Nowak, Phys. Rev. Lett. **117**, 107201 (2016).
[15] Z. R. Yan, Z. Y. Chen, M. H. Qin, X. B. Lu, X. S. Gao, and J.-M. Liu, Phys. Rev. B **97**, 054308 (2018).
[16] T. Shiino, S.-H. Oh, P. M. Haney, S.-W. Lee, G. Go, B.-G. Park, and K.-J. Lee, Phys. Rev. Lett. **117**, 087203 (2016).
[17] S. K. Kim, D. Hill, and Y. Tserkovnyak, Phys. Rev. Lett. **117**, 237201 (2016).
[18] Z. Y. Chen, Z. R. Yan, Y. L. Zhang, M. H. Qin, Z. Fan, X. B. Lu, X. S. Gao, and J.-M. Liu, New J. Phys. **20**, 063003 (2018).
[19] P. Wadley, S. Reimers, M. J. Grzybowski, C. Andrews, M. Wang, J. S. Chauhan, B. L. Gallagher, R. P. Campion, K. W. Edmonds, S. S. Dhesi, F. Maccherozzi, V. Novak, J. Wunderlich, and T. Jungwirth, Nat. Nanotechnol. **13**, 362 (2018).
[20] D. A. Allwood, G. Xiong, C. C. Faulkner, D. Atkinson, D. Petit, and R. P. Cowburn, Science **309**, 1688 (2005).
[21] S. S. P. Parkin, US Patent No. 6,834,005 (2004).
[22] S. S. P. Parkin, M. Hayashi, and L. Thomas, Science **320**, 190 (2008).
[23] L. Thomas, M. Hayashi, X. Jiang, R. Moriya, C. Rettner, and S. S. P. Parkin, Nature (London) **443**, 197 (2006).
[24] L. Thomas, M. Hayashi, X. Jiang, R. Moriya, C. Rettner, and S. Parkin, Science **315**, 1553 (2007).
[25] M. Hayashi, L. Thomas, C. Rettner, R. Moriya, X. Jiang, and S. S. P. Parkin, Phys. Rev. Lett. **97**, 207205 (2006).
[26] H. Y. Yuan and X. R. Wang, Phys. Rev. B **89**, 054423 (2014).
[27] S. Moretti, M. Voto, and E. Martinez, Phys. Rev. B **96**, 054433 (2017).
[28] E. Martinez, L. Lopez-Diaz, O. Alejos, L. Torres, and C. Tristan, Phys. Rev. Lett. **98**, 267202 (2007).
[29] E. Martinez, L. Lopez-Diaz, O. Alejos, and L. Torres, Phys. Rev. B **77**, 144417 (2008).
[30] D. Ravelosona, D. Lacour, J. A. Katine, B. D. Terris, and C. Chappert, Phys. Rev. Lett. **95**, 117203 (2005).
[31] D. Bedau, M. Kläui, M. T. Hua, S. Krzyk, U. Rüdiger, G. Faini, and L. Vila, Phys. Rev. Lett. **101**, 256602 (2008).
[32] H. Y. Yuan and X. R. Wang, Phys. Rev. B **92**, 054419 (2015).
[33] E. G. Tveten, T. Muller, J. Linder, and A. Brataas, Phys. Rev. B **93**, 104408 (2016).
[34] K. M. Pan, L. D. Xing, H. Y. Yuan, and W. W. Wang, Phys. Rev. B **97**, 184418 (2018).
[35] See Supplemental Material at http://link.aps.org/supplemental/10.1103/PhysRevB.100.020402 for details on the derivation of the depinning field and the movie on the motion of the domain wall for various α, where the color represents the magnitude of n_z.
[36] O. Gomonay, M. Kläui, and J. Sinova, Appl. Phys. Lett. **109**, 142404 (2016).
[37] J. J. Liang, J. H. Yu, J. Chen, M. H. Qin, M. Zeng, X. B. Lu, X. S. Gao, and J.-M. Liu, New J. Phys. **20**, 053037 (2018).
[38] K.-J. Kim, S. K. Kim, Y. Hirata, S.-H. Oh, T. Tono, D.-H. Kim, T. Okuno, W. S. Ham, S. Kim, G. Go, Y. Tserkovnyak, A. Tsukamoto, T. Moriyama, K.-J. Lee, and T. Ono, Nat. Mater. **16**, 1187 (2017).
[39] S. K. Kim, Y. Tserkovnyak, and O. Tchernyshyov, Phys. Rev. B **90**, 104406 (2014).
[40] P. Wadley, V. Hills, M. R. Shahedkhah, K. W. Edmonds, R. P. Campion, V. Novák, B. Ouladdiaf, D. Khalyavin, S. Langridge, V. Saidl, P. Nemec, A. W. Rushforth, B. L. Gallagher, S. S. Dhesi, F. Maccherozzi, J. Železný, and T. Jungwirth, Sci. Rep. **5**, 17079 (2015).